Contents lists available at ScienceDirect

Heliyon

Research article

Preliminary geochemical characterization of saline formation water from Miocene reservoirs, offshore Niger Delta

Taiwo A. Bolaji [a,b,*], Michael N. Oti [c], Mike O. Onyekonwu [d], Taiwo Bamidele [e], Michael Osuagwu [e], Leo Chiejina [f], Precious Elendu [e]

[a] World Bank African Centre for Excellence in Oilfield Chemicals Research, Institute of Petroleum Studies, University of Port Harcourt, Nigeria
[b] Department of Geology, Federal University Oye-Ekiti, Nigeria
[c] Department of Geology, University of Port Harcourt, Nigeria
[d] Department of Petroleum Engineering, University of Port Harcourt, Nigeria
[e] Shell Petroleum Development Company of Nigeria, Port Harcourt, Nigeria
[f] Shell Nigeria Exploration and Production Company, Lagos, Nigeria

ABSTRACT

The Niger Delta is one of the most prolific hydrocarbon provinces in the world, but information on basinal hydrogeology is scanty. Oilfield brines from nine producer wells in the Miocene reservoirs (2,472.25–3,532.48 m.b.s.l.), offshore Niger Delta, have been investigated along with two seawater samples to understand their hydrogeochemical characteristics in relation to the host rock mineralogy. Chemical analysis revealed that the waters are slightly alkaline and can be generally classified as saline water of the Na–Cl type based on their total dissolved solids (TDS). On the basis of bicarbonate, chloride, and sulphate ions, they are shown to be of connate origin. Relative abundance of major ions is in the following order: Na > Ca > Mg > K and Cl > HCO_3 > SO_4. Saturation indices (SI) of selected mineral phases calculated using PHREEQC indicate that the dissolution of iron oxide and carbonate minerals may contribute major ions in the formation water. The preponderance of alkali elements suggests the presence of feldspars, which could have resulted from sediments through which the water flows. An inverse relationship is observed between the resistivity of formation water and its TDS, which could be used to calculate resistivity values of formation waters in the area if the TDS contributions are known. Chemical data suggest that the formation waters were derived from seawater, dominantly altered by reverse ion-exchange processes and subsequently by water-rock interactions. Multivariate statistical analyses (correlation and factor analysis) indicate multiple sources of enrichment of ions in the formation waters.

1. Introduction

Oilfield brines or saline formation water, generally referred to as deep formation water in this paper, accompany the production of crude oil and/gas from reservoirs in sedimentary environments. Most oil and gas wells produce a saline solution, or brine, in addition to the desired oil and gas (Collins, 1975). Strictly speaking, the term "brine" refers to water with more than 35,000 mg/L (about 3.5 percent) total dissolved solids (TDS) (Hem, 1985). In terms of their origin, formation water may be connate – trapped in the pore space of sediment at the time of its deposition, or meteoric – derived from the atmosphere and percolated down through the vadose zone. Deep formation waters play an important role in many geological processes, such as metal mineralization, hydrocarbon

migration and accumulation, and diagenesis of rocks (Cathles and Smith, 1983; Land et al., 1988; Buzek and Michalíček, 1997). A thorough understanding of processes active during the evolution of sedimentary basins emerges when diagenetic studies of sedimentary rocks are integrated with geochemical trends in subsurface waters (Moldovanyi and Walter, 1992; Land, 1995). Hydrogeochemical studies of the chemical properties of formation waters and their relationship with local/regional geology help in resolving several problems associated with oilfield development and production. The chemical constituents of formation waters are derived from water-rock interactions as well as the dissolution and balance of the ionic composition in the water column (Cortes et al., 2016).

The Niger Delta has attracted the attention of numerous researchers due to its long history in oil and gas production, but the focus of most of

---

these studies is on several aspects of geology with scanty information on the basinal hydrogeology in published works of literature. Despite the availability of suitable data in the archives of oil companies operating in the region (Amajor and Gbadebo, 1992), the lack of investigation on formation waters in the basin may partly be due to the lack of access to oil facilities and confidentiality issues. This study seeks to describe and understand the hydrogeochemical characteristics of deep formation waters of the Freeman field in relation to the host rock mineralogy using the major ion distribution and multivariate statistical analysis.

1.1. Materials and methods

1.1.1. Location, geologic and tectonic setting

The area of investigation is a deep-water field, which lies on the continental slope of the Niger Delta basin, about 120 km offshore, southwest of Warri with water depths of about 1,000–1,200m (Figure 1). The seafloor in this area lies within the extensional and translational zone of Damuth (1994). The Niger Delta basin covers an area of over 70,000 km^2 and is composed of an overall regressive clastic sequence reaching a thickness of about 10,000–12,000 m composed of Quaternary and Tertiary sedimentary deposits. The Tertiary section of the Niger Delta is divided into three stratigraphic units – the Akata, the Agbada, and the Benin formations, representing prograding depositional facies distinguishable on the basis of sand-shale ratio. The type sections of these formations are designated as the Akata-1, Agbada-2, and Elele-1 wells respectively, located around Port Harcourt (Short and Stauble, 1967; Avbovbo, 1978). The Akata Formation (the oldest stratigraphic unit) located at the base of the delta is a deep marine pro-delta unit composing mainly shales deposited during the Paleocene. This formation is composed of thick shale sequences (potential source rock), turbidite sand (potential reservoirs in deep water) and minor amounts of clay and silt (Okiwelu and Ude, 2012). The paralic Agbada Formation, which is Eocene to Recent in age, consisting mainly of sequences of sandstones and shales overlies the Akata Formation. This unit constitutes the hydrocarbon reservoir while the shales form the seal. The Benin Formation (Eocene – Recent) deposited under continental fluviatile conditions is the topmost unit, consisting mainly of sands, which serve as a regional

aquifer. The deposition of the three formations occurred in each of the five off-lapping siliciclastic sedimentation cycles (depobelts) defined by synsedimentary faulting that occurred in response to variable rates of subsidence and sediment supply. The origin of the Niger Delta basin is associated with the evolution of a triple junction rift – ridge system that initiated the separation of the South American Plate in the late Jurassic (Whiteman, 1982; Weber and Daukoru, 1975). This separation was followed by early Cretaceous subsidence of the African margin. Marine sedimentation took place in the Benue Trough and the Anambra Basin as from Mid Cretaceous onwards. The Niger Delta started to evolve in the early Tertiary times, when clastic river inputs increased. Sediments were directly supplied from the weathering flanks of outcropping continental basement through the Niger-Benue drainage system (Burke et al., 1971; Whiteman, 1982; Stacher, 1994).

1.1.2. Sampling and analysis

Field sampling operations were undertaken in May and June 2017. Freshly produced fluid (oil and water) mixtures were sampled from nine production wells targeting Miocene reservoirs with a depth ranging from 2,472.25 – 3,532.48 m.b.s.l., collected via fitting sampling valves at the wellhead, into sterile metallic containers and shipped to the laboratory. No replication was conducted. The formation water was separated from the crude fraction using a separating funnel and was transferred into sterile Nalgene bottles, filled and covered to the brim and covered with airtight caps to minimize exposure to air. The Nalgene bottles were pre-cleaned, acid-washed (with 10% HNO_3), and thoroughly rinsed first with distilled water and then with Milli-Q deionised water. Before sample collection, these bottles were rinsed three times with the water to be sampled. The physical parameters of pH, redox potentials (Eh), and electrical conductivity (EC) were measured *in-situ* immediately after sample collection. The samples were stored in a portable cooler with ice packs during sampling and refrigerated at 4 °C upon arrival in the laboratory until analysis.

Major ion concentrations of the formation water samples were determined in accordance with Standard Methods for Examination of Water and Wastewater (APHA, 2013). Filtration of water samples
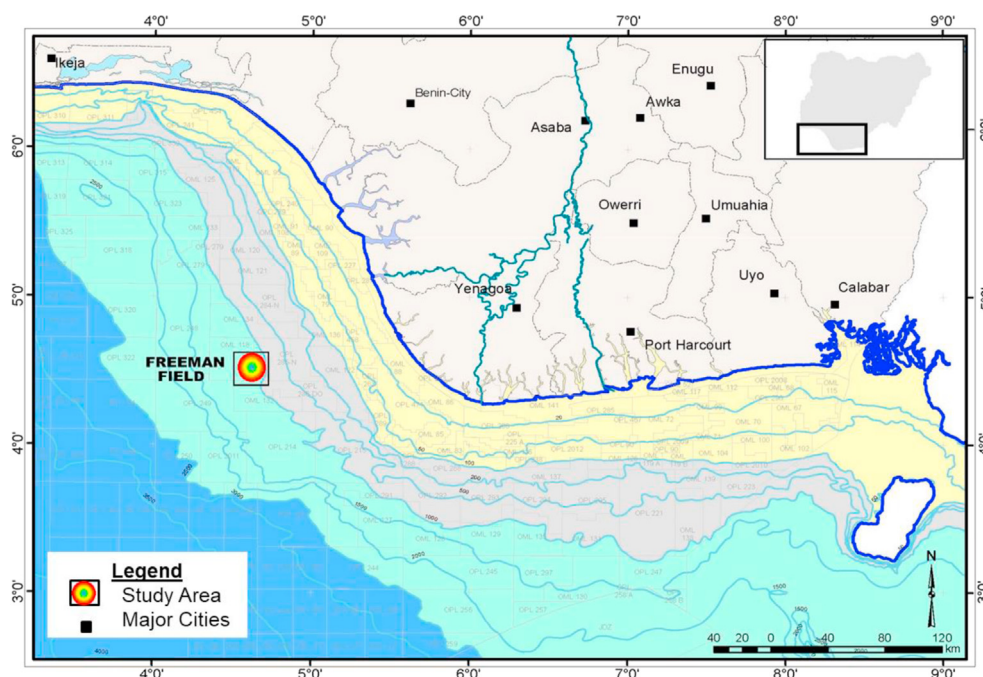
Figure 1. The Niger Delta continental margin showing the location of the study area (Bolaji, 2020).
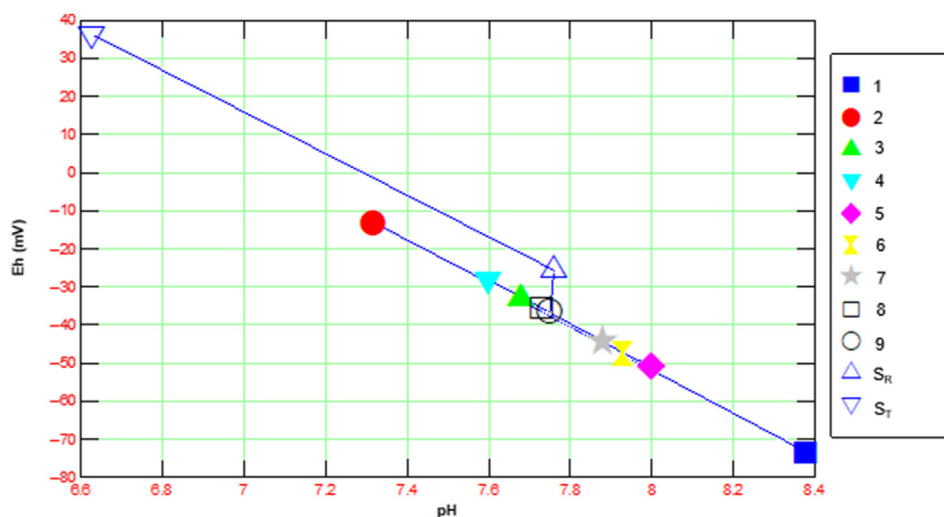
Figure 2. Eh–pH relationship for the studied water samples.

through a 0.45μm filter was done for the determination of anions and cations as suggested by Lico et al. (1982). pH and Eh were measured at 25 °C using the Orion Star A21PH/ISE meter and the YSI Model 3200 Conductivity Instrument was used to measure Electrical Conductivity. Sulphide was determined by Iodometric method; ammonium by Titration method; phosphate by Ascorbic acid method; chloride by Argentometric titration; total hardness (TH), calcium, and magnesium were determined using Complexometric titration techniques; Titrimetry and potentiometric principles were used to determine carbonate, bicarbonate and alkalinity; TDS was determined by Gravimetry method; sulphate and nitrate were measured using DR 6000 Spectrophotometer HACH-8051, while potassium, sodium and iron were determined using the GBC Scientific SavantAA Atomic Absorption Spectrophotometer (AAS). To measure how well the variance of each constituent can be explained by relationships with each other, correlations between major ions were determined using Pearson's correlation analysis (IBM SPSS 20 software).

Bivariate plots were used for identification of major processes while chloro-alkaline indices (CAI) were calculated to understand the base ion exchange reactions. Saturation indices (SIs) were calculated using the geochemical software PHREEQC (Parkhurst and Appelo, 1999) with the

MINTEQv.4 as the main database. Chemical equilibrium for selected mineral species can be examined by calculating the SI, which is expressed as:

$$SI = Log(IAP)/Ksp \tag{1}$$

where IAP is the Ion Activity Product representing the chemical activities of the dissolved ions of the mineral and Ksp stands for equilibrium constant (Eq. (1)).

The formation water is in thermodynamic equilibrium with the mineral phase, when the SI value is equal to 0. SI value is >0, when the water is oversaturated, resulting in mineral precipitation, while SI value <0 shows that the water is undersaturated, indicating that dissolution is required to reach equilibrium. The SIs of minerals such as anhydrite, aragonite, calcite, goethite, gypsum, halite, hematite, magnetite, and siderite were evaluated by the geochemical program PHREEQC.

1.2. Results and discussion

1.2.1. Water chemistry

Analytical results and statistical summary of the measured chemical parameters for formation waters from the Freeman oilfield are displayed

Table 1. Chemical composition of formation waters from Miocene-age reservoirs, Freeman field Niger Delta.

No.	*pH	*Eh	EC	Ca^{2+}	Mg^{2+}	Na^+	K^+	Fe_{tot}	Cl^-	SO_4^{2-}	HCO_3	NO_3	PO_4^{3-}	TH	TA	Salinity	TDS
		mV	mS/cm	mg/L	mg/L	mg/L	mg/L	mg/L	mg/L	mg/L	mg/L	mg/L	mg/L	mg/L	mg/L	‰	mg/L
1	8.38	-73.40	23.80	368.74	797.04	4,450.53	53.47	14.00	9,712.67	400.00	1415.20	7.20	0.33	4200.00	1160.00	17.547	17,671.43
2	7.32	-13.20	32.98	657.32	233.28	7,742.67	55.00	5.73	12,956.49	1100.00	1268.80	18.10	0.74	2600.00	1040.00	23.407	23,984.00
3	7.68	-33.30	39.49	545.09	349.92	13,328.00	61.13	12.93	12,043.30	600.00	1415.20	17.50	0.70	2800.00	1160.00	21.757	22,246.00
4	7.60	-28.10	30.73	432.86	806.76	7,974.67	46.67	17.27	13,313.82	1000.00	1122.40	6.10	0.28	4400.00	920.00	24.053	23,568.00
5	8.00	-50.80	40.03	561.12	1117.80	10,772.00	135.67	9.60	18,761.21	2000.00	927.20	19.10	0.85	6000.00	760.00	33.894	31,761.00
6	7.93	-47.50	35.67	737.47	330.48	7,561.33	112.27	8.20	15,672.24	1300.00	2147.20	6.70	0.36	3200.00	1760.00	28.313	28,430.00
7	7.88	-44.20	32.89	689.38	408.24	7,686.67	97.40	14.80	13,480.58	600.00	1512.80	16.80	0.67	3400.00	1240.00	24.354	24,043.00
8	7.73	-35.70	19.39	416.83	330.48	3,748.93	38.93	9.40	7,693.72	400.00	1756.80	12.00	0.61	2400.00	1440.00	13.899	14,617.00
9	7.75	-36.50	19.50	601.20	121.50	3,576.33	43.47	10.60	7,211.32	500.00	1464.00	12.70	0.63	2000.00	1200.00	13.028	14,537.00
Min.	7.32	-73.40	19.39	368.74	121.50	3576.33	38.93	5.73	7211.32	400.00	927.20	6.10	0.28	2000.00	760.00	13.03	14537.00
Max.	8.38	-13.20	40.03	737.47	1117.80	13328.00	135.67	17.27	18761.21	2000.00	2147.20	19.10	0.85	6000.00	1760.00	33.89	31761.00
Mean	7.81	-40.30	30.50	556.67	499.50	7426.79	71.56	11.39	12316.15	877.78	1447.73	12.91	0.57	3444.44	1186.67	22.25	22317.49
Std Dev.	0.29	16.74	7.90	128.83	329.17	3234.79	34.67	3.63	3705.44	530.98	353.59	5.24	0.20	1244.10	289.83	6.69	5866.06
S_R	7.76	-25.60	59.55	426.45	1240.27	10,067.00	194.00	268.00	21,071.83	2450.00	439.20	-	-	6168.00	360.00	38.068	36,184.00
S_T	6.63	36.20	59.20	391.18	1281.10	9,013.50	160.50	216.50	21,278.29	2300.00	217.16	-	-	6248.00	178.00	38.441	34,658.00

* Measured at 25 °C, S_R = Raw Seawater, S_T = Treated Seawater, TH = Total Hardness, TA = Total Alkalinity

in Table 1. The overall formation water pH, Eh and EC values (measured at 25 °C) in the study area ranges from 7.32 to 8.38, – 0.0734 to – 0.0132 mV, and 19.39 to 40.03 mS/cm respectively. The formation water samples presented slightly alkaline pH condition (average 7.81), while pH values of 7.76 and 6.63 were obtained for the raw seawater (S_R) and treated seawater (S_T) samples respectively. The pH and Eh of formation waters are important parameters influencing the solubility of minerals (Demir, 1995). The Eh–pH relationship for the studied water samples (Figure 2) suggests a reducing environment of marine waters and is represented by the equation Eh = – 0.0569 (pH) + 0.4041. TDS in the formation water vary between 14,537 and 31,761 mg/L ($Av.$ 22,317 mg/L) while 36,184 and 34,658 mg/L were obtained for S_R and S_T samples. This is consistent with the electrical conductivity (EC) value >19 mS/cm, with an average of 30.50 mS/cm for formation water samples and 59–60 mS/cm for seawater samples. Formation water TDS concentration is generally below that of seawater samples. The Alkalinity ranges between 760 and 1760 mg/L ($Av.$ 1186 mg/L) suggesting the existence of dynamic water-rock interaction. Alkalinity values of 178 and 360 mg/L were obtained for S_R and S_T respectively. Total hardness presents an average value of 3444 mg/L, mainly due to the abundance of magnesium rather than calcium. In seawater samples, TH slightly exceeds the peak value of 6,000 mg/L obtained for formation water samples. Chloride, bicarbonate and sulphate have the greatest concentrations among the anions. Chloride shows an average of 12,316 mg/L while bicarbonate displays an average of 1,447 mg/L. Sulphate concentration ranges between 400 and 2000 mg/L ($Av.$ 877 mg/L). This sulphate concentration could be associated with reduction of sulphate by organic matter as described by (Eq. (2); Appelo and Postma, 2005).

$$SO_4^{2-} + 2CH_2O \rightarrow H_2S + 2HCO_3^- \qquad (2)$$

Alkaline metals (*e.g.* Na$^+$, K$^+$) and alkaline earth metals (*e.g.* Ca^{2+}, Mg^{2+}) primarily occur in solution as ion pairs with Cl$^-$ (Drever, 1988), thus, it is appropriate to analyse cation concentrations and its distribution as chloride compounds (Hanor, 1994; Worden, 1996). The analyses revealed that Na$^+$ ($Av.$ 7,427 mg/L) is the dominant cation, while Cl$^-$ ($Av.$ 12,316 mg/L) is the dominant anion. Such high concentrations of Na and Cl ions confirm marine origin or suggest that the water has been caught up in a marine depositional environment with progressively high dissolution of halite in the formation. This is in accordance with analyses of formation waters from sedimentary basins around the world (Hanor, 1994) and consistent with results obtained in oilfield brines of the Eastern, Niger Delta (Amajor and Gbadebo, 1992). The Miocene sands of the Freeman field are predominantly quartz arenites, sub-arkoses and sub-litharenites, with typical framework composition Q$_{91}$, F$_5$, L$_3$ and they are typically fine to medium-coarse grained on the average (Bolaji, 2020). Since the dominant lithology in the area is clastic rocks, K-feldspar and mica dissolution may contribute K$^+$, Mg^{2+}, and HCO$_3^-$, which could be described as follows (Eqs. (3) and (4)):

$$4KAlSi_3O_8 + 4CO_2 + 22H_2O \rightarrow Al_4(Si_4O_{10})(OH)_8 + 8H_4SiO_4 + 4K^+$$
$$+ 4HCO_3^- \qquad (3)$$

$$4KMg_3AlSi_3O_{10}(OH)_2 + 28CO_2 + 30H_2O$$
$$\rightarrow Al_4(Si_4O_{10})(OH)_8 + 8H_4SiO_4 + 4K^+ + 28HCO_3^- + 12Mg^{2+} \qquad (4)$$
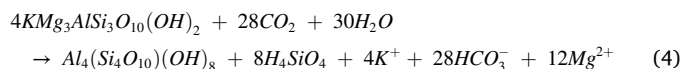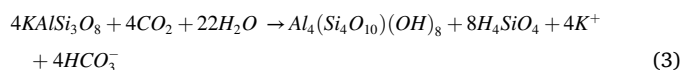
while dissolution of halite could serve as an important sources of Na^+ and Cl^- as described (Eq. (5)) below:

$$NaCl \rightarrow Na^+ + Cl^- \qquad (5)$$

TDS refers to the total amount of solids (mg/L) remaining when a sample of water is evaporated to dryness (Drever, 1988). This residual mass, called the residual TDS, represents the sum of all dissolved constituents. In this study, TDS is taken to be equivalent to the term "salinity". Both terms are used interchangeably here. TDS in the Freeman reservoirs are classified as hard saline water (Sawyer et al., 1994). Iron concentration in the formation water is generally below 18 mg/L, although we obtained 268 mg/L from the analysed S_R sample. The low nitrogen (N)-charge is attributed to the low NO$_3^-$ and NH$_4^+$ concentrations. Two reference samples, raw (S_R) and treated (S_T) seawater from around the facility are equally characterized as Na–Cl water types, with TDS concentrations of 36, 184 and 34, 658 mg/L respectively. The water resistivity (R_w)–TDS relationship (Figure 3) was established as follows: Log R_w = –4.94 ln (TDS) + 9.7621 at 25 °C, suggesting that electrical resistivity increases as TDS decreases, probably due to post-depositional processes and the inhomogeneous geological conditions in the reservoirs. This equation (R^2 = 0.90) can be used to calculate water resistivity values of other formation waters in the Freeman field for which the TDS values are available. Resistivity values (R_w) are for formation waters at 25 °C. There is no specific relationship between TDS and depth in the Freeman field contrary to the conclusions of Dickey et al. (1987) that TDS increases with depth. This may be attributed to the lithologies through which the waters moved which is predominantly sands and shales. The relative abundance of the major ions in formation water is in the following order: Na > Ca > Mg > K and Cl > HCO$_3$ > SO$_4$ > NO$_3$; whereas, ionic abundance in the seawater is as follows: Na > Mg > Ca > K and Cl > SO$_4$ > HCO$_3$.

1.2.2. Hydrogeochemical processes

Formation water chemistry often reflects the mineralogical composition of their host reservoirs and may provide important clues about diagenetic history of sedimentary basins with implications for oil exploration and production. The relationship between the major ions is useful for correlation and also in characterizing the origin of salts and hydrogeochemical processes (Hem, 1985). Cation exchange is one of the important geochemical processes, which significantly influences the evolution of hydrochemical characteristics of natural waters especially in detrital sedimentary environments. This process involves a reaction in which the calcium and magnesium in the water are exchanged for sodium that was adsorbed to reservoir solids such as clay minerals, resulting in higher sodium concentrations. It occurs as ion-exchange or reverse ion exchange (Eqs. (6) and (7)), and the probable reaction can be expressed as follows (Appelo and Postma, 2005):

$$2Na + (Ca_{1-x}Mg_x) - X \rightarrow (1-x)Ca + xMg + Na_2 - X \qquad (0 \leq x \geq 1) \qquad (6)$$
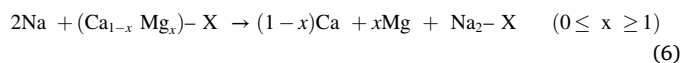
where X indicates the exchanging solid surface. The reverse process is represented as:

$$(1-x)Ca + xMg + Na_2 - X \rightarrow (Ca_{1-x}Mg_x) - X + 2Na \quad (0 \leq x \leq 1) \qquad (7)$$
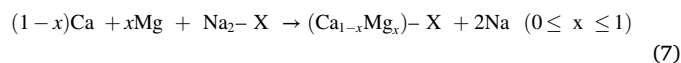
The relative contributions of the major weathering and dissolution mechanisms (silicate, carbonate, and evaporite) to the ion concentrations
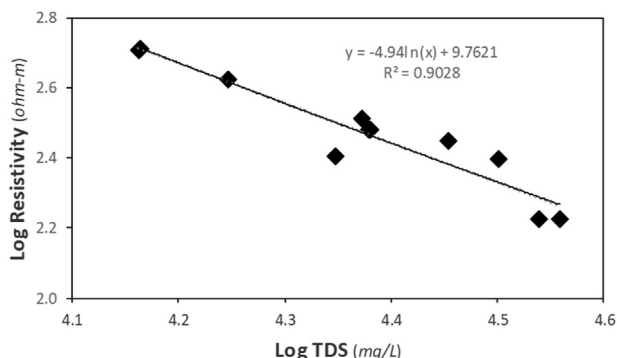
Figure 3. Relationship between formation water resistivity (R_w) and TDS.

Table 2. Ionic ratios computed for the formation water samples.

No.	Na/Cl	Ca/Mg	SO$_4$/Cl	Ca/SO$_4$	Ca/Cl	Ca/HCO$_3$	Mg/HCO$_3$	SO$_4$/HCO$_3$
1	0.707	0.281	0.030	2.210	0.067	0.793	2.827	0.359
2	0.921	1.709	0.063	1.432	0.090	1.578	0.924	1.102
3	1.706	0.945	0.037	2.178	0.080	1.173	1.241	0.539
4	0.924	0.325	0.055	1.038	0.058	1.174	3.608	1.132
5	0.885	0.304	0.079	0.672	0.053	1.843	6.052	2.740
6	0.744	1.353	0.061	1.360	0.083	1.046	0.773	0.769
7	0.879	1.024	0.033	2.754	0.090	1.388	1.355	0.504
8	0.751	0.765	0.038	2.498	0.096	0.722	0.944	0.289
9	0.765	3.001	0.051	2.882	0.147	1.250	0.417	0.434
Av	**0.920**	**1.079**	**0.050**	**1.891**	**0.085**	**1.219**	**2.016**	**0.874**
>1	1	4	0	8	0	7	5	3
>1%	11	44	0	89	0	78	56	33
<1	8	5	9	1	9	2	4	6
<1%	89	56	100	11	100	22	44	67
S$_R$	0.737	0.209	0.086	0.417	0.036	2.957	14.177	7.086
S$_T$	0.659	0.185	0.081	0.408	0.033	5.485	29.616	13.454

S$_R$ = Raw Seawater, S$_T$ = Treated Seawater.
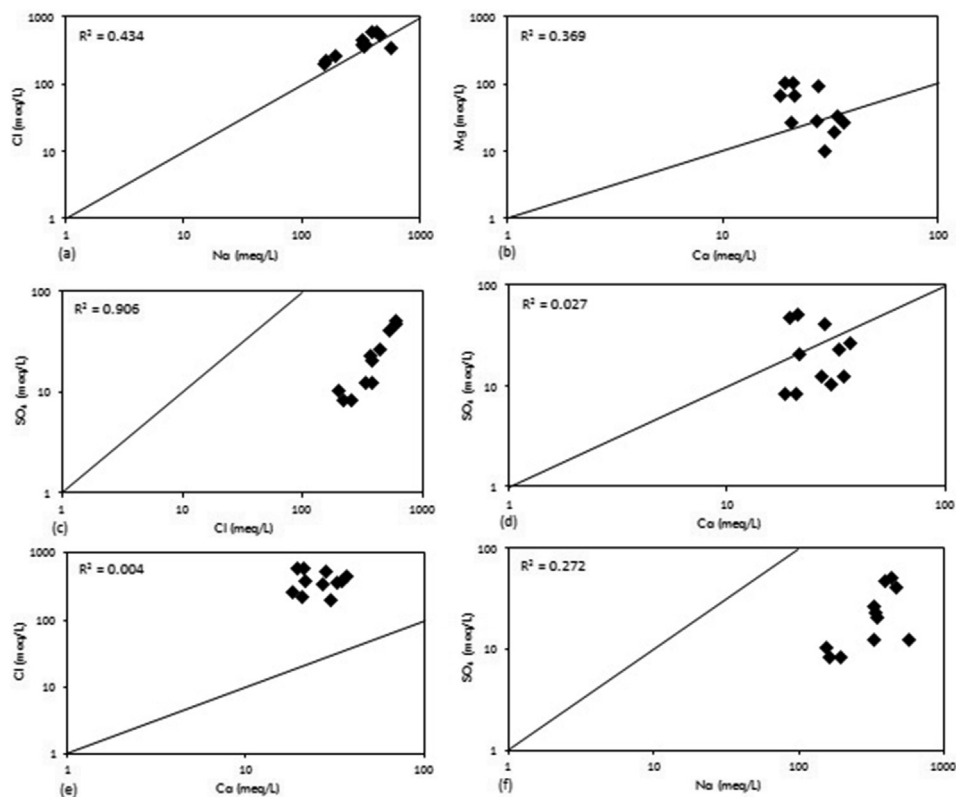
Figure 4. Ionic relationship to estimate hydrogeochemical processes in the studied formation water.

in the formation waters can be identified using selected molar ratio models. Based on the local geology of the study area, only silicate weathering (Gaillardet et al., 1999) was tested in this study. Silicate weathering is a geochemical process which results from the weathering of primary silicate minerals, resulting in the formation of clay minerals such as montmorillonite and kaolinite as its end product. The presence of Na and K in natural waters is attributed to the weathering of silicate minerals which may be derived from common igneous rocks.

Results obtained from the chemical analyses were used to identify the geochemical processes and mechanisms in the formation waters. Ionic

ratios were calculated (Table 2), and X–Y scatter plots are constructed between different component pairs (Figure 4). The sodium-chloride imbalance in the water is expressed by the Na/Cl ratio. Water is meteoric when this ratio is greater than unity and marine when it is less than unity (usually about 0.8). Most of the water samples investigated (89%) are below unity (Table 2), *i.e.* of marine origin. The Na/Cl ionic ratio for the seawater samples show a similar trend. In the same way, most of the formation water samples appear above the unit line (Figure 4a). The correlation coefficient is 0.687 (Table 3). Chloride excess could be related to reverse ion exchange process. The Ca/Mg ionic ratio, which is

Table 3. Correlation matrix of 15 variables computed from chemical data.

	pH	Eh	EC	Ca	Mg	Na	K	Cl	SO$_4$	HCO$_3$	NO$_3$	PO$_4$	TH	TA	TDS
pH	1.000														
Eh	-1.000**	1.000													
EC	-0.113	0.109	1.000												
Ca	-0.292	0.291	0.459	1.000											
Mg	0.493	-0.488	0.332	-0.448	1.000										
Na	-0.202	0.200	0.931**	0.261	0.284	1.000									
K	0.338	-0.334	0.700*	0.541	0.432	0.477	1.000								
Cl	0.047	-0.047	0.879**	0.430	0.556	0.687*	0.865**	1.000							
SO$_4$	-0.052	0.056	0.684*	0.356	0.536	0.500	0.767*	0.892**	1.000						
HCO$_3$	0.127	-0.133	-0.241	0.327	-0.603	-0.345	-0.018	-0.266	-0.343	1.000					
NO$_3$	-0.339	0.339	0.421	0.356	-0.080	0.494	0.288	0.251	0.248	-0.423	1.000				
PO$_4$	-0.312	0.316	0.302	0.338	-0.104	0.370	0.293	0.190	0.277	-0.360	0.970**	1.000			
TH	0.462	-0.456	0.480	-0.230	0.973**	0.376	0.610	0.716*	0.675*	-0.572	0.005	-0.026	1.000		
TA	0.127	-0.133	-0.241	0.327	-0.603	-0.345	-0.018	-0.266	-0.343	1.000**	-0.423	-0.360	-0.572	1.000	
TDS	0.001	-0.002	0.895**	0.495	0.483	0.697*	0.857**	0.996**	0.886**	-0.216	0.253	0.189	0.654	-0.216	1.000

** Correlation is significant at the 0.01 level (2-tailed).
* Correlation is significant at the 0.05 level (2-tailed).
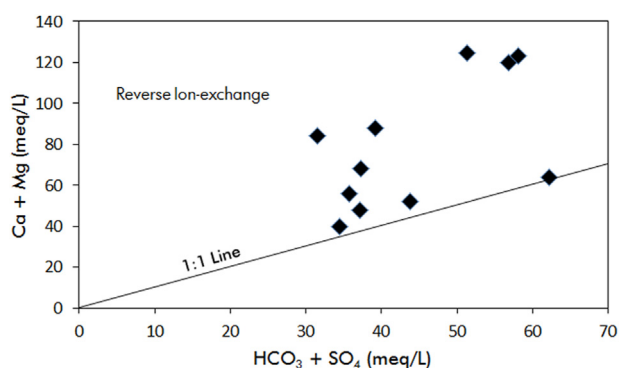
Figure 5. Ca + Mg *vs.* HCO$_3$ + SO$_4$ plot indicating reverse ion-exchange processes.

strongly influenced by the activity of base-exchange processes, helps in tracing seawater contamination (*for seawater* ≈ 0.21). This ratio is below unity in 56% of the formation water samples, indicating minimal marine influence (Table 2). Overall, for the formation waters the ratios are scattered in the binary plot (Figure 4b) with a weak negative correlation coefficient (–0.448) (Table 3).

Dissolution of halite, gypsum, or anhydrite dissolution may be determined by the SO$_4$/Cl ratio. The SO$_4$/Cl ratio is below unity (Table 2) for all formation water samples, reflecting the abundance of seawater in the deepwater reservoirs, similar to values obtained for seawater samples. Points on the SO$_4$/Cl binary plot for the water samples (Figure 4c) are clustered below the 1:1 equiline, where a strong positive relation (0.892) exist between SO$_4$ and Cl ions (Table 3), indicating a common provenance, probably seawater. Conversely, 89% of the waters analysed have Ca/SO$_4$ ratios above unity. The plotted samples (Figure 4d) are scattered mostly below the 1:1 line, showing a weak positive relationship (0.356, Table 3), indicating the addition of calcium due to weathering of calcium-rich minerals. The Ca/SO$_4$ ionic ratio computed for seawater samples indicates depletion of calcium.

The Ca/Cl ratio, which aids in studying the modification of water composition due to leaching and dissolution of different salts, is less than unity in all of the samples (Table 2), clustering above the 1:1 line (Figure 4e) on the Ca–Cl binary plot, with a weak correlation coefficient (0.430) showing the dominance of marine water in the reservoirs.

Bicarbonate is weakly correlated with Ca (0.327), while negative correlation (–0.603) exist between HCO$_3$ and Mg (Table 3). Significant Ca/HCO$_3$ ratios for most of the water samples (78%) and Mg/HCO$_3$ ratios in (56%) of the water (Table 2) suggest marine origin. Silicate weathering and reverse ion exchange of Ca and Mg with Na might be

Table 4. Descriptive statistics of saturation indices (SI) and Chloro-Alkaline Indices (CAI) computed for the water samples.

No.	SI_Anhydrite	SI_Aragonite	SI_Calcite	SI_Goethite	SI_Gypsum	SI_Halite	SI_Hematite	SI_Magnetite	SI_Siderite	CAI$_1$	CAI$_2$
1	-1.48	1.76	1.94	5.59	-1.24	-3.14	13.58	20.74	1.57	0.29	1.44
2	-0.80	0.98	1.16	2.88	-0.57	-2.77	8.16	12.65	-0.01	0.07	0.42
3	-1.21	1.28	1.46	3.81	-0.97	-2.55	10.03	15.44	0.55	-0.71	-4.08
4	-1.07	1.01	1.19	3.89	-0.83	-2.74	10.18	15.65	0.61	0.07	0.48
5	-0.72	1.37	1.55	4.21	-0.48	-2.44	10.82	16.60	0.36	0.11	0.79
6	-0.72	1.80	1.98	4.20	-0.48	-2.70	10.81	16.60	0.88	0.25	1.13
7	-1.06	1.61	1.79	4.42	-0.82	-2.75	11.25	17.25	0.98	0.11	0.70
8	-1.34	1.37	1.55	4.24	-1.10	-3.31	10.89	16.71	1.08	0.24	0.80
9	-1.06	1.48	1.66	4.35	-0.82	-3.36	11.11	17.03	1.09	0.23	0.80
S$_R$	-0.73	0.72	0.90	5.32	-0.50	-2.42	13.05	19.75	1.23	-	-
S$_T$	-0.78	-0.72	-0.54	2.91	-0.55	-2.46	8.23	12.60	-0.24	-	-
Min	-1.48	-0.72	-0.54	2.88	-1.24	-3.36	8.16	12.60	-0.24	-0.71	-4.08
Max	-0.72	1.80	1.98	5.59	-0.48	-2.42	13.58	20.74	1.57	0.29	1.44
Mean	-1.00	1.15	1.33	4.17	-0.76	-2.79	10.74	16.46	0.74	0.07	0.27

responsible for such high values. The Na relationship with SO_4 is significant (0.500) where sodium increase corresponds to sulphate (Figure 4f) while a weak correlation coefficient exists with Ca (0.261) and Mg (0.284), respectively (Table 3), which suggests water mixing.

The plot of Ca + Mg vs. HCO_3 + SO_4 (Figure 5) is a major indicator of ion-exchange processes (Cerling et al., 1989; Fisher and Mullican, 1997; Papazotos et al., 2019). Samples along the 1:1 equiline reveal dissolution of gypsum, calcite and dolomite. The right side of the plot is favoured if ion exchange is taking place due to an excess of HCO_3 + SO_4. Alternatively, a shift to the left showing slight dominance of Ca + Mg over HCO_3 + SO_4 indicates reverse ion exchange as the prevailing process. The high concentration of Ca + Mg (Figure 5) relative to HCO_3 + SO_4 can be as a result of reverse ion exchange in the study area. Most of the water samples are clustered around and above the 1:1 equiline, due to a deficiency of SO_4 and HCO_3, and an increase in Ca and/or Mg released by rocks, indicating the dominance of reverse ion exchange. The source of Ca and Mg in the samples was determined from m (Ca + Mg)/HCO_3 ratio (Sami, 1992). When the m (Ca + Mg)/HCO_3 is ($\geq$0.5), mineral (carbonate or silicate) weathering is responsible, while values below 0.5 indicate depletion of Ca and Mg relative to HCO_3 due to ion-exchange or enrichment of HCO_3. In this study, very high m (Ca + Mg)/HCO_3 ratios (ranging from 1.7–7.9) are observed, thus indicating that silicate weathering and reverse ion exchange are the prevailing hydrogeochemical processes.

The chemical reactions in which ion exchange between water and reservoir environment occurs during its travel or residence in the subsurface (Schoeller, 1967), usually encourage ion exchange and reverse ion exchange processes by the reservoir rock-fluid interactions (Berhe et al., 2017). Base exchange reactions (Eqs. (8) and (9)) between water and its host rock can be understood by studying the variation between the two Chloro-Alkaline Indices – (CAI_1 and CAI_2):

$$CAI_1 = \frac{(Cl^- - (Na^+ + K^+))}{Cl^-} \tag{8}$$

$$CAI_2 = \frac{(Cl^- - (Na^+ + K^+))}{SO_4^{2-} + HCO_3^- + CO_3^- + NO_3^-} \tag{9}$$

formulated by Schoeller (1967), where the concentration of ions is in meq/L. If Ca and Mg in the water is exchanged with Na and K in the host rocks, both indices are negative, whereas a reverse ion exchange gives positive indices (Nagaraju et al., 2006; Celik et al., 2008). In this study, CAI_1 values range from –0.71 to 0.29 with mean of 0.07, while CAI_2 values range from –4.08 to 1.44 with mean value of 0.27 (Table 4). In both cases, the resulting values indicate that samples show positive indices in 88.9% of the samples (Table 4) which further confirms reverse

ion exchange (Schoeller, 1967) as the dominant process, while 11.1% showed negative ratios indicating an indirect base-exchange reaction.

The thermodynamic equilibrium of sulphates (anhydrite, gypsum), carbonate (calcite, aragonite, and siderite), halide (halite), and iron oxide (goethite, hematite, and magnetite) was further examined using the geochemical software PHREEQC (Table 4). In this study, water samples were oversaturated with respect to iron oxide minerals and saturated by carbonate minerals, whereas samples are generally undersaturated for halide and sulphide minerals. The mineral phases that are oversaturated (SI > 0) will precipitate out of solution. Therefore, the dissolution of iron oxide and carbonate minerals may contribute major ions in the formation water of Freeman field. High concentration of iron is associated with the presence of Fe^{2+} from dissolution of Fe-bearing minerals in the reservoirs, which eventually gets oxidized to Fe^{3+} by redox dynamics.

1.2.3. Origin of the brines

The Cl–SO_4–HCO_3 ternary plot, which according to Dickey (1966) and De Sitter (1957), is the best genetic discriminant of meteoric and connate formation waters, revealed that the formation waters associated with this oilfield are characteristically high in chloride and low in carbonate. The ternary plot of these anions shows a cluster towards the Cl apex (Figure 6a). Therefore, it is believed that these waters are predominantly pure connate waters. This is evidenced in the similarity of major ionic ratios of the formation waters and seawater (Table 2). On the (Na + K)–Mg–Ca ternary plot (Figure 6b), the formation waters cluster around the (Na + K) pole, reflecting the dominance of alkali elements, with a reasonable proportion of Ca and Mg ions, which suggests the presence of carbonates and probably detrital igneous and metamorphic sediments along the flow paths of these waters. The high Na + K values suggest the presence of feldspars in the sediments through which the formation waters flow. This is consistent with the subsurface geology of the Niger Delta.

1.3. Statistical analysis

1.3.1. Correlation between variables

Using principal component analyses based on the Eigen analysis of the correlation matrix, the correlation coefficients were determined in order to pinpoint relationships between variables, which serve as indicators of the overall coherence of the data, contributions of each chemical parameter, and measure of the extent of variability between each individual pair. Pairs showing the dependency of one parameter on the other give high positive correlation (Sharma and Sharma, 2011). Initial information about the correlation structure of the data was obtained from the correlation matrix of the 15 variables (Table 3). Correlations fluctuate from –0.018 (for K vs. HCO_3 and TA) to 1.000 (correlation between HCO_3 and TA). Only correlation coefficients larger
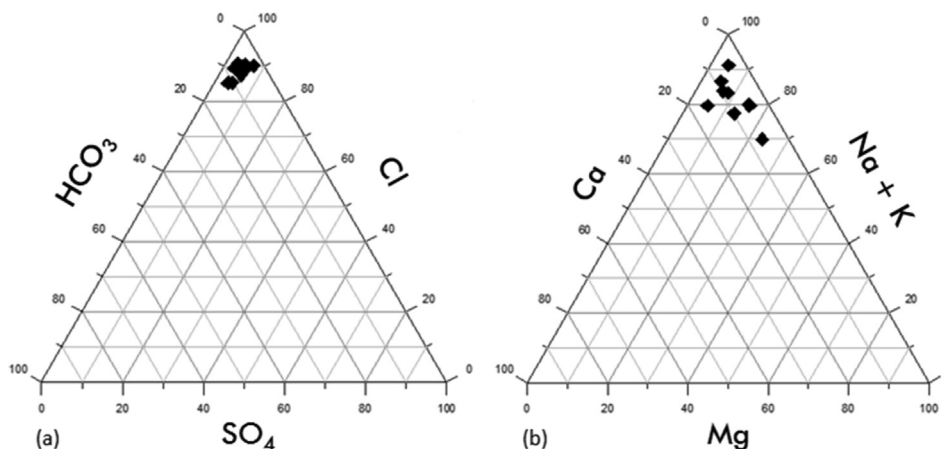
Figure 6. Ternary plots for the studied formation waters (a) Cl–SO_4–HCO_3, (b) (Na + K)–Mg–Ca.

Table 5. Rotated factor loading matrix, eigenvalues, % variance, and cumulative variance values.

Parameter	Factor			
	1	2	3	4
pH	-0.018	-0.021	0.976	-0.161
Eh	0.018	0.015	-0.974	0.163
EC	0.905	-0.070	-0.112	0.191
Ca	0.521	0.646	-0.223	0.343
Mg	0.430	-0.726	0.481	-0.198
Na	0.718	-0.205	-0.217	0.265
K	0.847	0.136	0.424	0.235
Cl	0.982	-0.133	0.081	0.041
SO4	0.869	-0.218	0.011	0.070
HCO3	-0.143	0.922	0.112	-0.272
NO3	0.208	-0.141	-0.191	0.942
PO4	0.149	-0.096	-0.140	0.955
TH	0.603	-0.624	0.466	-0.127
TA	-0.143	0.922	0.112	-0.272
TDS	0.993	-0.066	0.031	0.042
Eigenvalue	6.498	3.534	2.656	1.263
% variance	43.322	23.559	17.709	8.420
Cumulative (%)	43.322	66.881	84.589	93.009

Extraction Method: Principal Component Analysis.
Rotation Method: Varimax with Kaiser Normalization.

than 0.500 were considered to have significant mutual correlation, while those below –0.500 rather involve indirect mutual correlation. A very strong positive correlation exists between Eh and pH, while a weak correlation exists between other variables (Table 3).

1.3.2. Factor analysis

Factor analysis (FA) was applied to 15 water quality parameters using IBM SPSS 20. Descriptive statistics of the water quality data are presented in Table 1. Factors extracted by principal component analysis gives a new
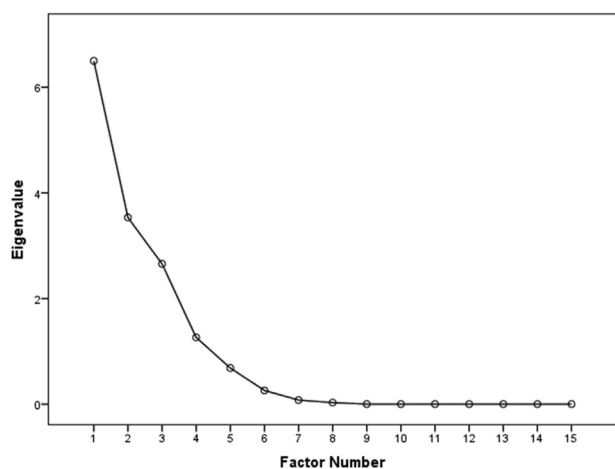
Figure 7. Scree plot of the eigenvalues.
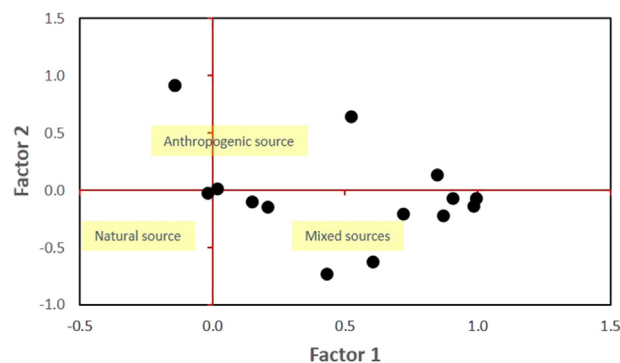
Figure 8. Source identification plot of factors 1 and 2.

Table 6. Total variance explained.

Component	Initial Eigenvalues			Rotation Sums of Squared Loadings		
	Total	% of Variance	Cumulative %	Total	% of Variance	Cumulative %
1	6.498	43.322	43.322	5.682	37.878	37.878
2	3.534	23.559	66.881	3.199	21.327	59.205
3	2.656	17.709	84.589	2.727	18.181	77.386
4	1.263	8.420	93.009	2.344	15.623	93.009
5	0.684	4.559	97.568			
6	0.259	1.729	99.298			
7	0.077	0.513	99.810			
8	0.028	0.190	100.000			

Extraction Method: Principal Component Analysis. Four (4) factors explained 93.0% of the total variance which is the total cumulative %.
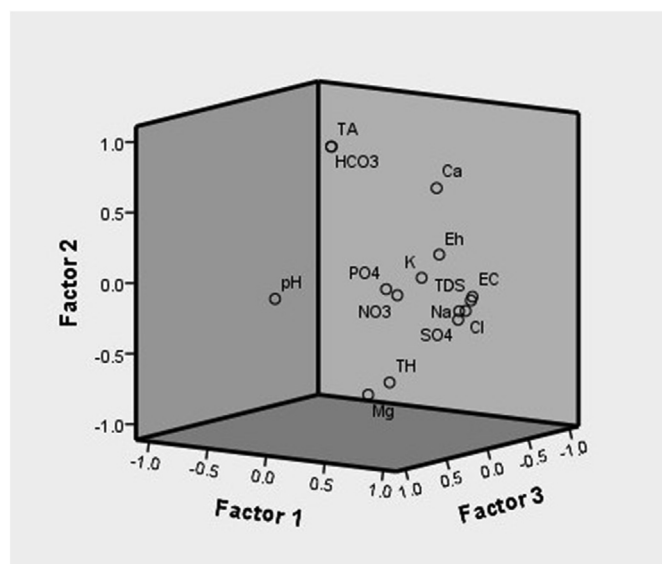
Figure 9. The loading plot of factor scores for the studied water samples.

rotated factor Varimax in which each factor is described in terms of only those variables obtained from water analysis for ease of interpretation. Table 5 shows that four-factor loadings explained 93.0% of the total variance, using the Varimax with Kaiser normalization, with Eigenvalues ≥ 1. From the result of the FA, the four Eigenvalues are greater than 1. An Eigenvalue gives a measure of the significance for the factor, and the highest value is the most significant.

The scree plot (Kaiser, 1960, Figure 7) reveals the Eigenvalues sorted from large to small as a function of factor number. Beyond the fourth factor (starting the elbow in the downward curve), other components could be omitted (Figure 7; Table 6). The scree plot explains that the first two factors (1 and 2) are more significant than the other two (3 and 4) as they represent about 67% of the total variance. The latter only account for about 26%.

The summary of the factor loadings, their Eigenvalues and their variances are shown in Table 6, in descending order depending upon the percentage of variance. The factor having the highest variance is assigned the first position, with the lowest variance in the fourth place. The following factors were indicated, considering the hydrogeochemical aspects of the water samples:

Factor 1: TDS, Cl, EC, SO$_4$, K, Na, TH and Ca
Factor 2: TA, HCO$_3$, Ca, and Mg
Factor 3: pH, and Eh
Factor 4: PO$_4$, and NO$_3$.

TDS, Cl, EC, SO$_4$, K, Na, TH, and Ca marked factor 1 explained 43.3% of the variance, giving high positive loading with values 0.993, 0.982, 0.905, 0.869, 0.847, 0.718, 0.603 and 0.521 respectively. This indicates a highly linear relationship between this factor and these parameters, which are thought to be responsible for the hydrogeochemical regimes in the formation waters. Factor 2 is strongly correlated with TA, HCO$_3$, Ca,

and Mg, which explained 23.6% of the variance. Factor loadings were 0.954, 0.954, 0.954, 0.585, and –0.688, respectively. The strong positive factor loading (referred to as the alkalinity factor) is usually due to the presence of bicarbonate, and it correlates very closely with calcium. The negative correlation with Mg may be due to reverse ion exchange processes and dissolution of silicate minerals.

To gain a better understanding of the derived dominant factors (1 and 2), a simplified bivariate plot was prepared (Figure 8) to deduce the prevailing sources of enrichment of ions in the formation waters. These could be natural, anthropogenic or mixed (water-rock interaction, anthropogenic influences, atmospheric contribution, seawater intrusion, and cation exchange processes) sources (Raju et al., 2016). According to the plot, ions (Ca, Mg, Na, K, SO$_4$, Cl, and HCO$_3$) and general parameters (TH, TA, TDS, and EC) are contributed by mixed (multiple) sources.

The following factor loadings 0.976, and –0.974, representing pH, and Eh are included in Factor 3, which accounts for 17.7% of the variance controls the solubility of minerals. The strong negative loading is indicative of the reducing environment of the formation waters. Finally, the fourth factor explained 8.4% of the variance with PO$_4$, and NO$_3$ having high positive loadings of 0.955, and 0.942 respectively. The high positive loading may be due to anthropogenic or metabolic activities of microorganisms within the reservoirs. Figure 9 shows the contributions of the different parameters towards the first three factors in the water samples. Factor scores for the studied formation water samples were calculated to obtain the level of contribution of each parameter as shown in Table 7.

1.4. Conclusion

This study is a preliminary investigation of the chemistry and hydrogeology of formation waters from Miocene siliciclastic reservoirs, offshore Niger Delta. Significant findings from this study have indicated that the formation waters are slightly alkaline, hard saline waters, primarily of Na–Cl water type. The concentration of these and other ions suggests that the formation waters were derived from seawater with subsequent alterations by water mixing, reverse ion exchange and silicate weathering as revealed by the ionic ratios and CAI indices. Saturation index (SI) of selected mineral phases calculated using PHREEQC geochemical software suggests that the dissolution of iron oxide and carbonate minerals may contribute major ions in the formation water. An inverse relationship is observed between the formation water resistivity and TDS, which is probably due to post-depositional processes and the inhomogeneous geological conditions. A mathematical relationship was established to calculate resistivity values of formation waters in the area if TDS is known. The relative abundance of the major ions is in the following order: Na > Ca > Mg > K = Cl > HCO$_3$ > SO$_4$ > NO$_3$. The formation waters are genetically classified as connate waters high in chloride, TDS and salinity, and low in resistivity and bicarbonate contents.

Co-evaluating geological and hydrogeochemical data from the Miocene reservoirs of the Freeman field through chemical analyses of formation water, hydrochemical bivariate plots of major ions, multivariate statistical analysis, and geochemical modelling has shown the effectiveness of these tools in interpreting formation water data, and establishing the factors and mechanisms that control its chemistry. The data presented here provide a cohesive methodological framework to assess formation water chemistry in oilfield reservoirs.

Declarations

Author contribution statement

Taiwo A. Bolaji: Conceived and designed the experiments; Performed the experiments; Analyzed and interpreted the data; Wrote the paper.

Michael N. Oti, Mike O. Onyekonwu: Conceived and designed the experiments; Wrote the paper.

Table 7. Factor scores.

Component	1	2	3	4
1	0.897	-0.349	0.094	0.255
2	0.062	0.345	-0.766	0.538
3	0.378	0.859	0.246	-0.244
4	-0.222	0.146	0.586	0.765

Taiwo Bamidele, Michael Osuagwu, Leo Chiejina, Precious Elendu: Contributed reagents, materials, analysis tools or data.

Data availability statement

Data included in article/supplementary material/referenced in article.

Declaration of interests statement

The authors declare no conflict of interest.

Additional information

No additional information is available for this paper.

References

Amajor, L.C., Gbadebo, A.M., 1992. Oilfield brines of meteoric and connate origin in the Eastern Niger Delta. J. Petrol. Geol. 15 (4), 481–488.

APHA, 2013. Standard Methods for the Examination of Water and Wastewater, 22nd (Ed.). American Public Health Association, Washington, D.C. Environment Federation.

Appelo, C.A.J., Postma, D., 2005. Geochemistry, Groundwater and Pollution, second ed. Balkema, Rotterdam.

Avbovbo, A.A., 1978. Tertiary lithostratigraphy of Niger delta. AAPG (Am. Assoc. Pet. Geol.) Bull. 62, 295–300.

Berhe, B.A., Dokuz, U.E., Celik, M., 2017. Assessment of hydrogeochemistry and environmental isotopes of surface and groundwaters in the Kutahya Plain, Turkey. J. Afr. Earth Sci. 134, 230–240.

Bolaji, T.A., 2020. Reservoir Souring Possibilities in Freeman Oilfield, Niger Delta: Insights from Mineralogy, Diagenesis and Water Chemistry. PhD Thesis of the University of Port Harcourt, Nigeria.

Burke, K., Dessauvagie, T.F.J., Whiteman, A.J., 1971. Opening of the Gulf of Guinea and geological history of Benue depression and Niger delta. Nat. Phys. Sci. (Lond.) 233, 51–55.

Buzek, F., Michalíček, M., 1997. Origin of formation water of the bohemian massif and Vienna basin. Appl. Geochem. 12, 334–343.

Cathles, L.M., Smith, A.T., 1983. Thermal constraints on the formation of Mississippi Valley-type lead -zinc deposits and their implications for episodic basin dewatering and deposit genesis. Econ. Geol. 78, 983–1002.

Celik, M., Unsal, N., Tufenkci, O.O., Bolat, S., 2008. Assessment of water quality of the lake seyfe basin, Kirsehir, Turkey. Environ. Geol. 55, 559–569.

Cerling, T.E., Pederson, B.L., Von Damm, K.L., 1989. Sodium–calcium ion exchange in the weathering of shales: implications for global weathering budgets. Geology 7, 552–554.

Collins, A.G., 1975. Geochemistry of Oilfield Waters. Elsevier, New York, p. 496.

Cortes, J.E., Munoz, L.F., Gonzalez, C.A., Nino, J.E., Polo, A., Suspes, A., Siachoque, S.C., Hernandez, A., Trujillo, H., 2016. Hydrogeochemistry of the formation waters in the San Francisco field, UMV basin, Colombia – a multivariate statistical approach. J. Hydrol. 539, 113–124.

Damuth, J.E., 1994. Neogene gravity tectonics and depositional processes on the deep Niger Delta continental margin. Mar. Petrol. Geol. 11 (3), 320–346.

De Sitter, I.C., 1957. Diagenesis of oilfield brines. AAPG Bull. 31, 2030–2040.

Demir, I., 1995. Formation Water Chemistry and Modeling of Fluid-Rock Interaction for Improved Oil Recovery in Aux Vases and Cypress Formations, Illinois Basin. Illinois State Geological Survey Report, p. 60.

Dickey, P.A., 1966. Patterns of chemical composition in deep subsurface waters. AAPG Bull. 50, 2472–2478.

Dickey, P.A., George, G.O., Barker, C., 1987. Relationships among oils and water compositions in Niger Delta. AAPG Bull. 71 (10), 1319–1328.

Drever, J.I., 1988. The Geochemistry of Natural Waters: Upper Saddle River, N.J. Prentice Hall, p. 437.

Fisher, S.R., Mullican, W.F., 1997. Hydrogeochemical evaluation of sodium-sulphate and sodium-chloride groundwater beneath the northern Chihuahua desert, Trans-Pecos, Texas, USA. Hydrogeol. J. 5 (2), 4–16.

Gaillardet, J., Dupre, B., Louvat, P., Allegre, C.J., 1999. Global silicate weathering and CO2 consumption rates deduced from the chemistry of large rivers. Chem. Geol. 159 (1), 3–30.

Hanor, J.S., 1994. Physical and chemical controls on the composition of waters in sedimentary basins. Mar. Petrol. Geol. 11, 31–45.

Hem, J.D., 1985. Study and Interpretation of the Chemical Characteristics of Natural Water, 2254. U.S. Geological Survey Water-Supply Paper, p. 264.

Kaiser, H.F., 1960. The application of electronic computers to factor analysis. Educ. Psychol. Meas. 20, 141–151.

Land, L.S., 1995. Na-Ca-Cl saline formation waters, Frio Formation (Oligocene), south Texas, USA: Products of diagenesis. Geochem. Cosmochim. Acta 59 (11), 2163–2174.

Land, L.S., Macpherson, G.L., Mack, L.E., 1988. Geochemistry of saline formation waters, Miocene, offshore Louisiana. AAPG (Am. Assoc. Pet. Geol.) Bull. 72 (9), 1115, 1115.

Lico, M.S., Kharaka, Y.K., Carothers, W.W., Wright, V.A., 1982. Methods for collection and analysis of geopressured geo-thermal and oil field waters. U.S. Geological Survey Water-Supply, p. 21. Paper 2194.

Moldovanyi, E.P., Walter, L.M., 1992. Regional trends in water chemistry, Smackover Formation, Southwest Arkansas: geochemical and physical controls. AAPG (Am. Assoc. Pet. Geol.) Bull. 76 (6), 864–894.

Nagaraju, A., Suresh, S., Killham, K., Hudson, E.K., 2006. Hydrogeochemistry of waters of mangampeta barite mining area, cuddapah basin, Andhra Pradesh, India. Turk. J. Eng. Environ. Sci. 30, 203–219.

Okiwelu, A.A., Ude, I.A., 2012. 3D modelling and basement tectonics of the Niger Delta basin from aeromagnetic data. In: Sharkov, Evgenii (Ed.), Tectonics – Recent Advances. IntechOpen.

Papazotos, P., Koumantakis, I., Vasileiou, E., 2019. Hydrogeochemical assessment and suitability of groundwater in a typical Mediterranean coastal area: a case study of the Marathon basin, NE Attica, Greece. HydroRes. 2, 49–59.

Parkhurst, D.L., Appelo, C.A.J., 1999. User's guide to PHREEQC (version 2)—a computer program for speciation, batch-reaction, one-dimensional transport, and inverse geochemical calculations. U.S. Geo. Survey Water Res. Invest. Rep. 99–4259, 312.

Raju, N.J., Patel, P., Reddy, B.S.R., Suresh, U., Reddy, T.V.K., 2016. Identifying source and evaluation of hydrogeochemical processes in the hard rock aquifer system: Geostatistical analysis and geochemical modeling techniques. Environ. Earth Sci. 75 (16), 1157.

Sami, K., 1992. Recharge mechanisms and geochemical processes in a semiarid sedimentary basin, Eastern Cape, South Africa. J. Hydrol. 139, 27–48.

Sawyer, C.L., McCarthy, P.L., Parkin, G.F., 1994. Chemistry for Environmental Engineering, fourth ed. McGraw-Hill Book Company, p. 545p.

Schoeller, H., 1967. Geochemistry of groundwater. In: An International Guide for Research and Practice, 15. UNESCO, pp. 1–18.

Sharma, P., Sharma, H.P., 2011. Groundwater quality assessment of Pachim Nalbari block of Nabari district Assam based on major ion chemistry. Int. J. Chem. Res. 3 (4), 1914–1917.

Short, K.C., Stauble, A.J., 1967. Outline of geology of Niger delta. Am. Assoc. Petrol. Geol. Bull. 51, 761–779.

Stacher, P., 1994. Niger delta hydrocarbon habitat. Nigeria Assoc. Petrol. Explo. Bull. 9/01, 67.

Weber, K.J., Daukoru, E., 1975. Petroleum geological aspects of the Niger delta. Nig. Journ. Min. Geol. 12, 9–32.

Whiteman, A.J., 1982. Nigeria: its Petroleum and Potentials, 1&2. Graham and Trotman, London, p. 394.

Worden, R.H., 1996. Controls on halogen concentrations in sedimentary formation waters. Mineral. Mag. 60, 259–274.